Landslides (2019) 16:2017–2032
DOI 10.1007/s10346-019-01216-5
Received: 7 February 2019
Accepted: 29 May 2019
Published online: 22 June 2019

Saima Riaz · Gonghui Wang · Muhammad Basharat · Kaoru Takara

Experimental investigation of a catastrophic landslide in northern Pakistan

Abstract The territory of Azad Jammu and Kashmir (AJK) is vulnerable to different natural hazards because of its proximity to a geodynamically active zone and its tropical and monsoonal climatic pattern. Both factors operate in various combinations and result in the occurrence of disasters generated by natural hazards like floods, earthquakes, and landslides at different intervals. There are numerous landslides in the study area, out of which the Donga Kass landslide has been selected for study due to its ongoing activity which poses a significant risk to the nearby community and infrastructure. Therefore, assessment of two possible triggering factors (i.e., earthquake and rainfall) for this landslide was conducted through the laboratory testing using the DPRI-5 Ring shear simulator. Undrained cyclic loading tests were performed to simulate the dynamic loading and earthquake-induced landslides, while pore pressure control tests simulated the rise of groundwater level during rainfall for rainfall-induced landslides. Based on the laboratory test results, a critical seismic acceleration and a critical pore pressure ratio are suggested for Donga Kass landslide. Using these values and combining with rainfall data and monitored pore water pressure in bore holes, early warning system can be activated to reduce any potential landslide risk in the future.

Keywords Donga Kass landslide · 2005 Kashmir earthquake · Cyclic ring shear test · Pore pressure control test

Introduction

Landslides can be considered a symptom of fragility, either natural or human-induced. A small seismic shock in a sensitive mountainous system can cause a landslide (Hufschmidt et al. 2005). The 2005 Kashmir earthquake (M = 7.6) was among the worst ever event to hit the region of AJK, Pakistan. The geographical location of Pakistan and Muzaffarabad is shown in Fig. 1a, b, respectively. In the case of AJK, a highly seismotectonic system received a great shock resulting in massive landslide damage. According to Earthquake Reconstruction and Rehabilitation Authority (EERA 2005), official death toll as of November 2005 stood at 87,350 out of which 26,500 fatalities were directly or indirectly related to landslides. Over time, a steady state will be reached once all active landslides reached to equilibrium stage through a reduction of slope angle or by exhausting all susceptible material (Hufschmidt et al. 2005; Petley et al. 2006). In the meantime, areas with cracks and active landslides will continue to pose a significant risk to communities.

Khattak et al. (2010) have surveyed the entire AJK and reported that all landslides are located near rivers and roads. It is estimated that almost all landmass of AJK is vulnerable to rainfall and earthquakes of different magnitudes which among other factors like deforestation, road construction etc. cause landslides on slopes. According to a study conducted by the Forestry Resource Department in AJK on existing damage, about 85% of landslides, upon failure, will have a direct impact on the infrastructure such as roads, electricity supply lines, houses, and rural pathways leading to villages. There are numerous landslides in the study area such as Panjgran, Ghori, Dhanni, Sandok, and Shahkot Landslides that are some of the major landslides in terms of size and susceptibility.

These landslides are frequently triggered by rainfall especially in the monsoon season which not only result in road closure and damage to private and public property but also loss of invaluable human lives. Muzaffarabad receives heavy rainfall during the monsoon season each year. The average rainfall for the Muzaffarabad is 1395 mm/year (average value from 2000 to 2017), with 30–60% in the form of snowfall during December–February, usually in the areas with an elevation more than 2000 m (AJK Planning and Development Department Report 2015). Figure 2a shows the annual rainfall patterns at Muzaffarabad station and cumulative number of landslides in District Muzaffarabad AJK, Pakistan from 2000 to 2017.

Precipitation data was obtained from the Pakistan metrological department, Lahore office, and landslide data was taken from the planning and development department, AJK. Figure 2b depicts the monthly rainfall patterns at Muzaffarabad station and number of landslides during monsoon season and dry season in District Muzaffarabad AJK, Pakistan from 2004 to 2008. It is shown that the monsoon season starts from July and ends at the end of August (heavy rainfall occurs with monthly extremes of up to 620 mm). In September, rainfall declines, and by November conditions are dry, with minimal rainfall of 30 mm/month. January to May is also dry months in the region.

The data shown in the Fig. 2a, b depicts that even before the 2005 Kashmir earthquake, there were many landslides during the monsoon season of the year 2004. During Kashmir earthquake in October 2005 (Fig. 2a), a number of landslides were triggered during the earthquake despite the fact that earthquake was hit the region in the dry season and subsequently drastically increased during the upcoming monsoon seasons of years 2006, 2007, and 2008 which is also described by Saba et al. (2010) and Konagai and Sattar (2011) in their studies. Out of those landslides, Donga Kass landslide was selected for study due to its ongoing activity and impact on the infrastructures (i.e., the Neelum road and the Donga Kass bridge which is the only link to a nearby village and it had been adversely affected by the event of landslide activation, see Fig. 4e, f and also often blocked the pathway to the adjacent village). The risk of landslide in the study area had been recognized by landslide susceptibility maps by the government of AJK and also by some researchers after the 2005 earthquake; however, detailed study to fully understand the possible initiation and movement mechanisms of the landslides in this area has not been undertaken; hence, there was a need to assess the landslide risk in this area based on the detailed field and laboratory investigation. To elevate our precision in the risk assessment, this experimental study for the catastrophic landslide in Northern Pakistan is unique and provides basic information from the geotechnical point of view.

Study area

The Donga Kass landslide is located approximately 6 km to the north of Muzaffarabad city along the main Neelum Valley road. The location of the landslide is shown in Fig. 1b. It is bounded by longitude

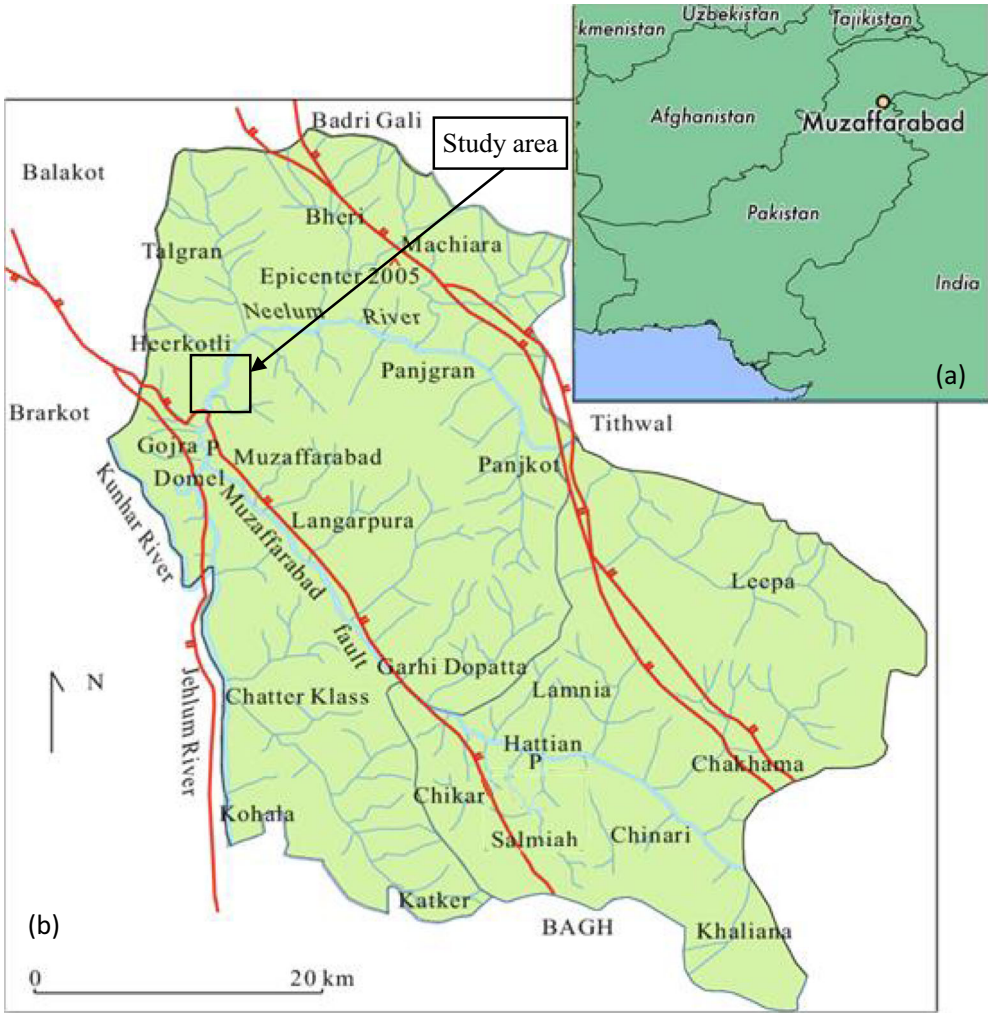

Fig. 1 **a** Geographical location of the study area (map of Muzaffarabad district digitized and modified after the map from Planning and Development department AJK 2015, Basharat et al. 2012). **b** The geographical location map of Pakistan. Approximately 26,500 fatalities can be directly or indirectly linked to the landslides induced during 2005 Kashmir earthquake (Petley 2006). The economic loss was assessed to be 5.2 billion US $ (ADB and WB 2005)

73° 28′ 53.75″ to 73° 29′ 04.91″ N and latitudes 34° 25′ 11.46″ to 34° 25′ 19.04″E. The Donga Kass landslide is the most dangerous and active landslide in the valley because it activates every year during the monsoon season. In this season, there are heavy thundershowers

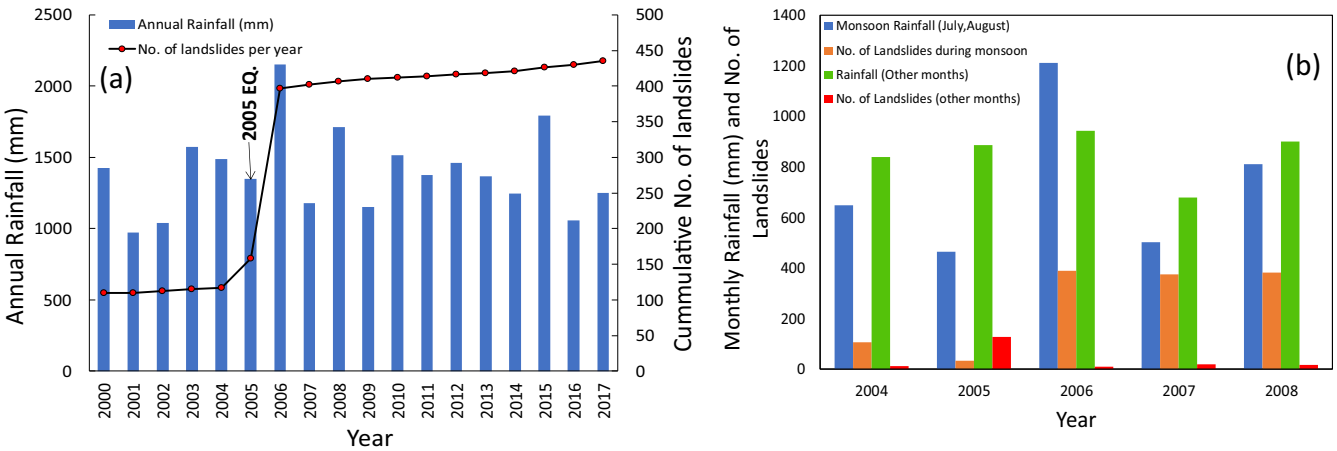

Fig. 2 **a** Annual rainfall characteristics at Muzaffarabad station with number of landslides triggered each year. **b** Monthly rainfall and number of landslides triggered each month in District Muzaffarabad AJK, Pakistan from 2004 to 2008

and strong gusty winds followed by flash floods. Monsoonal climate persists in Muzaffarabad with annual precipitation of ~ 1500 mm. Snow falls at altitudes of > 1500 m during winter.

The landslide was initially triggered by the October 8, 2005 (M 7.6) Kashmir earthquake and destroyed the Neelum Valley road and dammed the river temporarily. The landslide isolated the Kotla and Neelum Valley areas from the rest of the state of AJK, and other parts of Pakistan. The road remained blocked for a few weeks to vehicular traffic. It was reactivated on July 28, 2006 and triggered by a heavy rainstorm with 614 mm total rainfall and a maximum rate of rainfall of 102 mm/h. The landslide obliterated four houses and six shops in the nearby village close to Muzaffarabad, the capital of AJK and caused the death of three people. The Neelum Valley road winding through the mountainous region in northeast of Muzaffarabad was also blocked for traffic for more than a week, with long patches having been wiped out by rains.

The landslide had several episodes of reactivation in the past. The most recent landslide activation occurred on September 25, 2016 in which 17 people were killed and 3 were injured. The passengers were boarding in a bus, while passing through the landslide, the landslide activated, and debris started to flow and a big boulder dropped on the bus, the driver could not control the bus and fell down into the Neelum river. When the Deputy Commisioner (DC) of the Neelum district and other officials reached at the landslide spot to help the people, again it activated and a big boulder struck at them and DC died at the spot and other people injured.

At present, about a 200 m section of road near Donga Kass (Fig. 3) has been badly damaged by the landslide. An interdisciplinary approach is needed to understand and analyze the landslides, manage risks, and to develop an early warning system in the study area. Effective early warning systems for rainfall and earthquake-induced landslides must have strong meteorological, hydrogeological, and geotechnical components. Fortunately, meteorological monitoring, forecasting, and warning are developed in the Pakistan (an annual report is published by Planning and Development Department each year), but the research on the hydrogeological and geotechnical aspects of landslide early warning systems has not been done in the region. There is a lot of literature available related to the landslide susceptibility maps by using geospatial technology in the AJK, but research on geotechnical aspects is very rare. So, there was a dire need of in-depth geotechnical and geological investigation of active landslides in the AJK to bridge this gap.

At present, there is no early warning system in the study area, the government of AJK is in the process to develop such system and this study can contribute as the preliminary investigation for the study area. Rainfall thresholds can form the basis of landslide warning systems supplemented with the geotechnical investigation (direct observation of soil moisture and pore water pressure) it can provide a more reliable indicator of impending slope instability than indexes based on rainfall observations alone. This interdisciplinary approach to assessing landslides offers policy makers a more holistic picture of the underlying causes of landslides and an improved basis for designing a sustainable disaster risk reduction strategy.

Keeping in view this problem, the landslide was investigated to understand the causes and the failure mechanism. The purpose of the laboratory tests in current study (pore pressure control tests and cyclic stress control tests) is to investigate the most probable triggering factor for the Donga Kass landslide. It did not expect to solve the problems in the study area only by providing these test results, but this study can elevate the understanding on the landslide phenomena at the Donga Kass landslide.

Geological and tectonic characteristics of the donga Kass landslide

The Donga Kass landslide (Fig. 3) occurs in the Eocene Kuldana Formation. The Kuldana Formation consists of variegated shale, siltstone, sandstone, and highly fossiliferrous limestone lenses. The litho-stratigraphic units exposed at the locality of the landslide are shale and sandstone of the Kuldana Formation. The main lithological unit is composed of maroon splintery shale which is interbedded with thin beds of sandstone. The strike of the

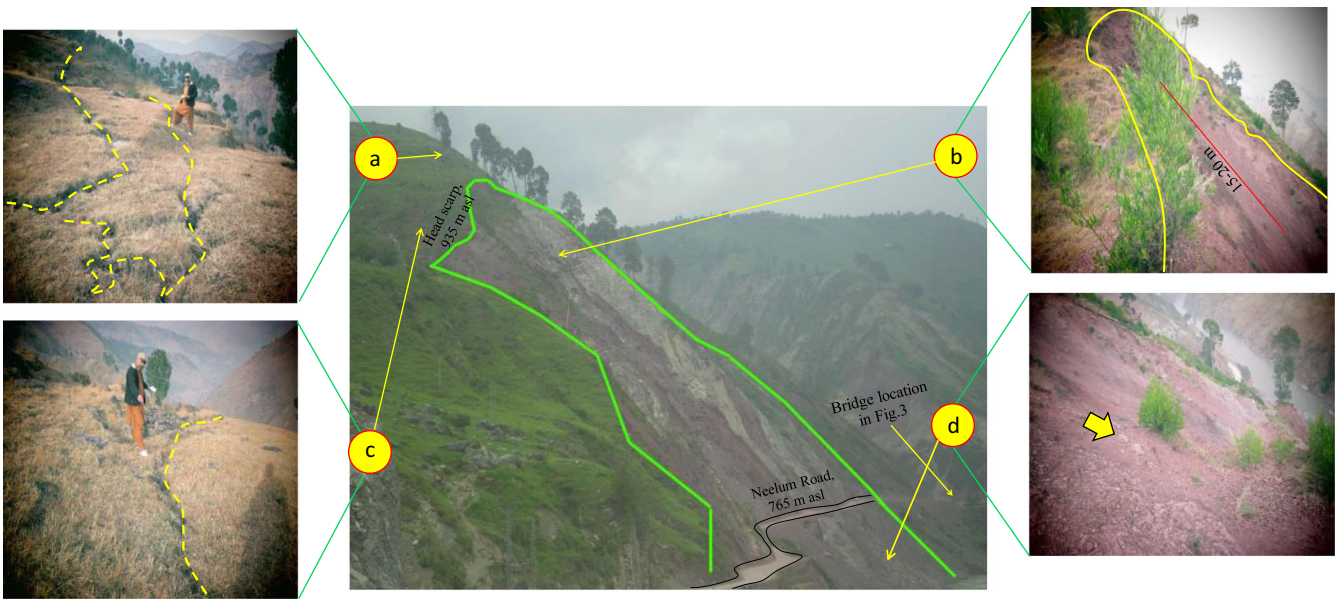

Fig. 3 Overview of the Donga Kass landslide

sandstone bed is trending from SW to NE and dipping in SE direction. The dip angle ranges from 70 to 80°. The main body of the landslide contains mainly shale fragments with abundant gravel, pebble, and cobble fractions of sandstone.

The study area lies in the Himalayan fold and thrust belt (Hazara Kashmir Syntax) which is seismically active region. The intense seismicity and active faults are well known in Himalayas (Basharat et al. 2017; Hussain et al. 2004). The Muzaffarabad Fault and the related active hanging wall anticline are the result of active deformation (Baig et al. 2008). This tectonic deformation caused uplift of the hanging wall block during many earthquakes and produced a significant fault scarp morphology, steep slopes, and a topographic front (Baig et al. 2008; Kaneda et al. 2008). The hanging wall block is highly fractured and jointed. Consequently, the brittle shear zone along the fault varies from 500 to 1000 m distance (Basharat et al. 2017).

Field investigation and landslide mapping

Three field visits were carried out for detail landslide mapping and soil samples collection. The first field visit was carried out in May 2016 for reconnaissance survey and to identify the active landslides along the Neelum road from the information given by the Planning and Development Department, Azad Jammu and Kashmir (AJK). Field investigation was carried out to understand the relationship between lithology, initiation of landslide, travel path, deposited area, and mapping of the scarp and body of the landslide. During the field visit, it was observed that Donga Kass landslide has tension cracks, fractures, and multiple secondary scarps (see Fig. 4) which can be reactivated in the future. The second field visit was carried out in September 2016 to document the landslides in detail. Moreover, the construction of the longitudinal and cross profiles was developed. The third field visit was carried out in March 2017 to collect the soil samples for laboratory testing. Global Positioning System (GPS), Laser Distance Meter, clinometer, Brunton compass, and tape measurement were used during the field investigation. Landslide photographs have been taken to document the landslide features.

Donga Kass landslide was mapped on scale 1:1200. The distinct lithological units have been identified and mapped. The lithological units and geological formations have also been presented on the maps with bedding attitude where available. Brunton compass was used to measure the attitude of beds. The landslide segments have been demarcated by taking GPS points in the field. The length and width of landslides were measured using Laser distance meter (Reigl-F-21 H) with an accuracy of $\pm$15 cm. The slope angle was measured by using clinometer. The field observations regarding landslides were also noted, during the field survey.

Longitudinal and cross profiles have been prepared by using the field data taken by laser distance meter shown in Fig. 4c, d. The profiles show the initiation of movement and the debris material exposed along the longitudinal and cross sections of the landslide. These longitudinal and cross profile have been used to understand the intact mass and the transported material along the landslide surface. The volume of landslides was roughly estimated by multiplying the landslide area with the average thickness. The thickness of the deposit was observed during field investigation and calculated from the construction of longitudinal and cross profiles. The total surface area and deposit area of landslides have been calculated using ArcGIS software after mapping.

The debris material moves from the source area and travels towards the valley floor. However, a large amount of debris material remains deposited at the middle and lower part of the main slide. In the middle portion of the slide just along the road and below the road, the sandstone exposures are present within the debris material. The bedrock sandstone, which is highly jointed and cracked with thick accumulated debris above, is exposed in the road cut. Thick to massive beds of shale are also exposed on both right and left flanks with two distinct beds of sandstone pinched between them. The right side of the slide is dominated by surficial material and sloping towards the valley. During field investigation, it was observed that big boulders had accumulated in the upper and middle parts of the slide. The thickness of debris material is greater below the road due to the dumping of material in the process of clearing the road from the sliding material. The area of the slide enlarges towards both flanks and towards the lower ends of the main body. Total surface area of the landslide was calculated to be about 26,500 m^2 (Fig. 5a). The elevation measured from top to toe is about 185 m and the landslide traveled the distance of 350 m towards the Neelum River. The total volume is about 0.16 million m^3 estimated by multiplying the average thickness with the covered area.

The landslide was initiated at the elevation about 935 m asl (above sea level) and traveled towards the Neelum River (Fig. 3a). The main scarp is the top most detached edge of the landslide from the original undisturbed ground surface. It developed by the failure of the softer shale material along the slope. The length of the main scarp varies along the circumference of the scarp.

Three sets of concentric cracks about 15 cm to 1.5 m wide and up to 1 m deep were observed above the landslide which extends 50 m above the top of the main scarp (Fig. 4b). The slope failure has damaged the agricultural terrace above the scarp (Fig. 4c). The affected area of the crown was measured at about 100 m long and 50 m wide. At the lower part of scarp near the main body of the slide, a sandstone bed (Fig. 4d) is exposed which pinches out in the shale bed towards the top. The head scarp of the landslide is nearly inclined (50–60°) with vertical height of 15–20 m. Similar to the head scarp, the left and right flank of the landslide is characterized by a steep slope and high cliff.

This landslide was triggered during the 2005 Kashmir earthquake and was reactivated in monsoon season of 2006, and the road was washed away into the Neelum river alongwith debris. After that, a retaining wall was constructed as a countermeasure and road was rebuilt. This landslide again reactivated during the monsoons of 2010, 2013, and 2016 and damaged the road; then, concrete was used to strengthen the existing road. The countermeasures were, however, ineffective. The retaining wall was observed to be tilting, with a displacement of about 5–10 cm, and there were many cracks on the road and concrete pavement, deformation, and subsidence was also observed on the road. The strata in the studied area are mainly bedded sandstone and shale. The slip surface of the landslide has the tendency to parallel the bedding plane within beds or lenses of shale.

Field observation showed that below the weathering crust about 1–5 m thick, on the upper sedimentary rocks layer, there are lot of vertical joints (fractures) and tilting trees (Fig. 4a, b). These fractures allow water and surface moisture to penetrate the rock and weaken sandstone, siltstone, and the shale layer, causing an increase in weight, reducing the bonding strength between two layers and thus promoting

Fig. 4 **a** Photograph showing the landslide initiation. **b** Tension cracks on the crown. **c** Agricultural land. **d** Exposed sandstone on the right flank. **e** Donga Kass bridge before landsliding in 2006. **f** Blockage of Neelum road due to debris and damage of deck slab of Donga Kass bridge after landsliding

failure. Regarding most of the landslide observed, the authors recognized that landslide was a translational type of slide and the slip surface had been covered by debris and did not expose, formed by displacement of sedimentary rocks over a weaker layer (e.g., mudstone or shale layer). The particular importance was the presence of shale layers within a landslide between sedimentary rocks (sandstone, siltstone) as shown in Fig. 5a, d. These can be some controlling factors (i.e., steep slope, presence of clayey material, construction of the Neelum road, and river under cutting along with rainfall and tectonic activity) causing landslides in the study area.

Depletion zone

The depletion zone of the landslide is defined as the area of landslide covered by the displaced material which lies below the main scarp as shown in Fig. 5b. The depletion zone of the Donga Kass landslide is 85–135 m wide and 55–95 m long. The rock mass in the source area consists of thick shale and fractured sandstone at the top. The displaced material forms an overhanging topography at various locations due to the presence of relatively competent sandstone beds beneath. The thick deposit of unconsolidated material along the traveling path increased the landslide volume. The material deposited in the depletion zone is finer than that in the transitional zone.

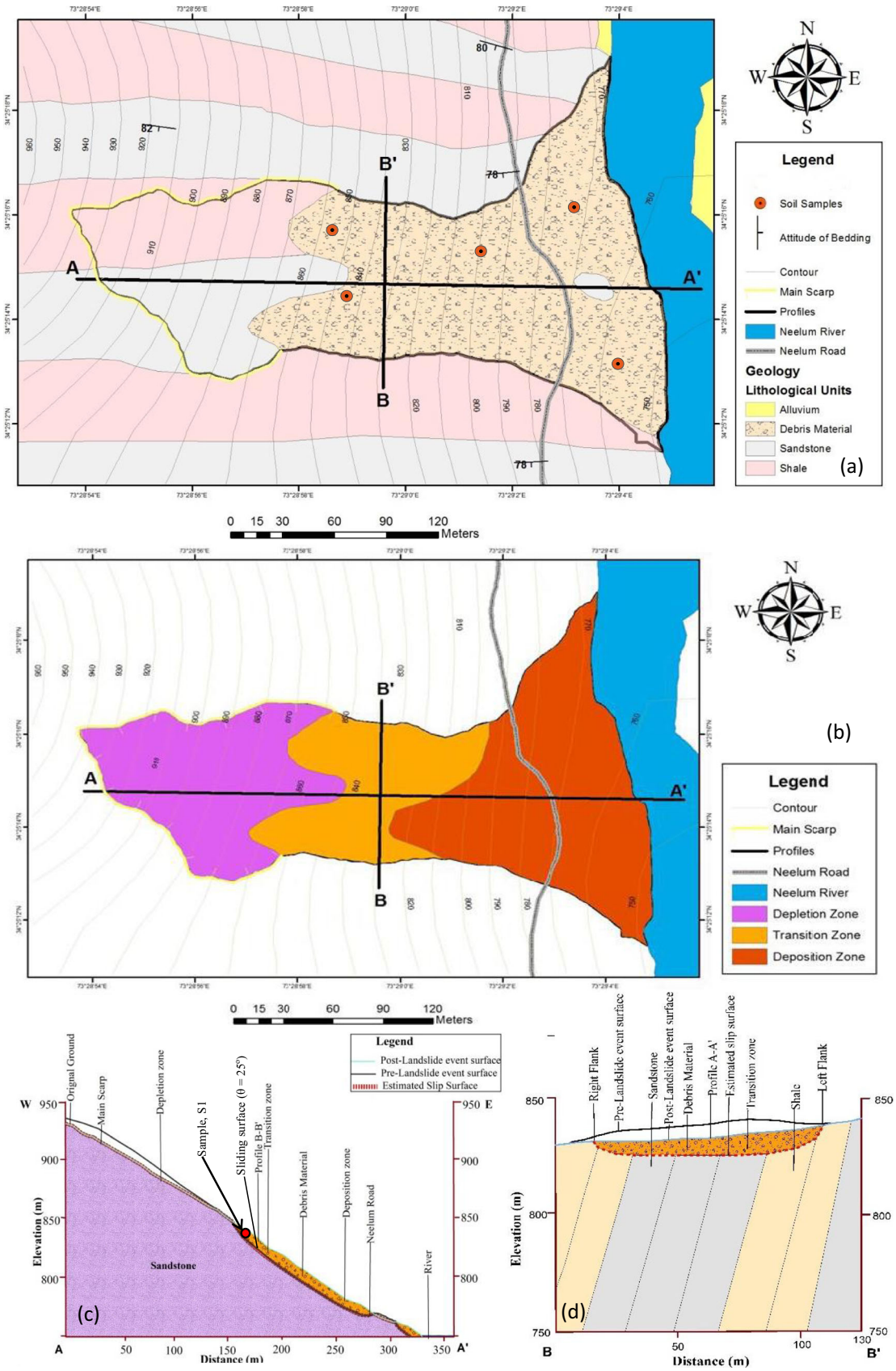

Fig. 5 **a** Geological units of the Donga Kass landslide and sampling location. **b** Map showing different zones of the Donga Kass landslide. **c** Cross section of the Donga Kass landslide. **d** Longitudinal profile of the Donga Kass landslide

Transition zone

The middle portion of the landslide body is the transition zone. It covers the major portion of the landslide. It lies between the depletion zone and depositional zone (Fig. 5b). The material is deteriorated from the depletion zone and deposited in this zone. The length of the transitional zone is 50–120 m and the width of this zone is 80–95 m. The total surface area of transition zone is about 6450 m^2. The average width of this zone is less than that of the depletion zone. The transitional zone can be divided into two segments on the basis of material and morphology. The upper portion is clay dominated while lower part contains coarser fractions. The slope angle measured in this zone was 30–40°. This zone can be characterized as a sandy zone. The lower zone of transition is above the depositional zone which is a coarser material zone. At this segment, fractured and crushed gray color sandstone is exposed.

Deposition zone

The zone of accumulation is the last zone (shown in Fig. 5b) where a major portion of the material is deposited. The accumulation zone of the landslide is 65–135 m long and 95–145 m wide. The total surface area of this zone is 10,500 m^2. It consists mainly of sandstone boulders with some fine material having been eroded by the Neelum river. The size of the soil particles is variable, and they range from sandstone boulders to fine clays. The proportion of boulders is greater than the debris material. The toe area mainly consists of sandstone boulders with some coarse soil fractions as the finer material was washed away by the river. The thickness of the landslide deposit is roughly estimated to be about 6–8 m as shown in Fig. 5c, d. The diameter of the boulders accumulated at toe ranges from 1 to 3 m.

Methodology

To investigate the landslide failure mechanism, five samples from a depth of 1 m by manual drilling with an auger were collected from the transported debris material (transition and deposition zones of the landslide as discussed above) above the Neelum valley road (Fig. 5a). Each sample was weighed 10 kg and was packed in airtight plastic bag. These samples were transported to University of Engineering and Technology Lahore to determine the index properties (Table 1) and grain size distribution curves (shown in Fig. 6). The figure shows that curves for all the samples are almost identical and index properties are also close to each other. Only one sample S1, weighed 10 kg, was transported to Japan for laboratory testing due to the limitation of weight from the custom and immigrations departments of Pakistan and Japan. The particle size distribution is set to pass through ASTM sieve no. 10 (the particles size diameter 2.00 mm). Donga Kass specimen (S1) has specific gravity of soil particles $G_s = 2.65$, maximum dry density $\rho_{dmax} = 2.05$ g/cm^3, minimum dry density $\rho_{dmin} = 1.55$ g/cm^3, mean grain size $D_{50} = 0.47$ mm, and uniformity coefficient $U_c = 7.15$. Donga Kass soil specimen has 4% fine fraction and is a non-plastic material. Ring shear tests were performed on the collected sample by using the landslide Ring shear simulator (DPRI-5) at the Disaster Prevention Research Institute (DPRI), Kyoto University. The ring-shear apparatus was designed initially to investigate the residual shear resistance mobilized along the sliding surface at large shear displacements in landslides because it allows unlimited deformation of the specimen. The test configuration for the ring-shear device was introduced by Hvorslev (1939); this concept was improved by Bishop et al. (1971), Bromhead (1979), Savage and Sayed (1984), Sassa (1984), Hungr and Morgenstern (1984), Tika (1989), and Garga and Sendano (2002).

The high-speed ring-shear apparatus (DPRI-1) developed by Sassa (1984) and his colleagues at Disaster Prevention Research Institute, Kyoto University used a conventional shear-speed control motor; it could not provide cyclic shear-stress loading. The first dynamic-loading ring-shear apparatus (DPRI-3) was developed to reproduce seismic loading using a torque-control motor and a servo-control system that utilized the feed-back signal from a load cell that measured torque (Sassa 1994, 1996). Following DPRI-3, a series of dynamic-loading ring-shear apparatus has been developed that incorporated different features (DPRI-4, DPRI-5, DPRI-6, and DPRI-7).

Table 1 Physical properties of the collected samples

	S1[a]	S2	S3	S4	S5
Specific gravity, *Gs*	2.65	2.67	2.66	2.65	2.66
Maximum dry density, ρ_{dmax} (g/cm^3)	2.05	–	–	–	–
Minimum dry density, ρ_{dmin} (g/cm^3)	1.55	–	–	–	–
Liquid limit, LL (%)	24.92	22.98	25.81	26.85	26.34
Plastic limit, PL (%)	–	–	23.06	24.78	–
Plasticity Index, PI (%)	NP	NP	2.74	2.02	NP
In situ moisture content (%)	8.5	10	9	11	11
Fine fraction (passing through sieve No. 200), F_s (%)	4	5	5	7	6
Average particle size, D_{50} (mm)	0.47	0.5	0.5	0.60	0.61
Effective particle size, D_{10} (mm)	0.095	0.09	0.11	0.095	0.10
Coefficient of uniformity (C_u)	7.15	7.11	6.18	8.63	8.20
Coefficient of curvature (C_c)	0.82	0.84	0.70	1.0	1.09

[a] Sample S1 was transported to Japan for laboratory testing

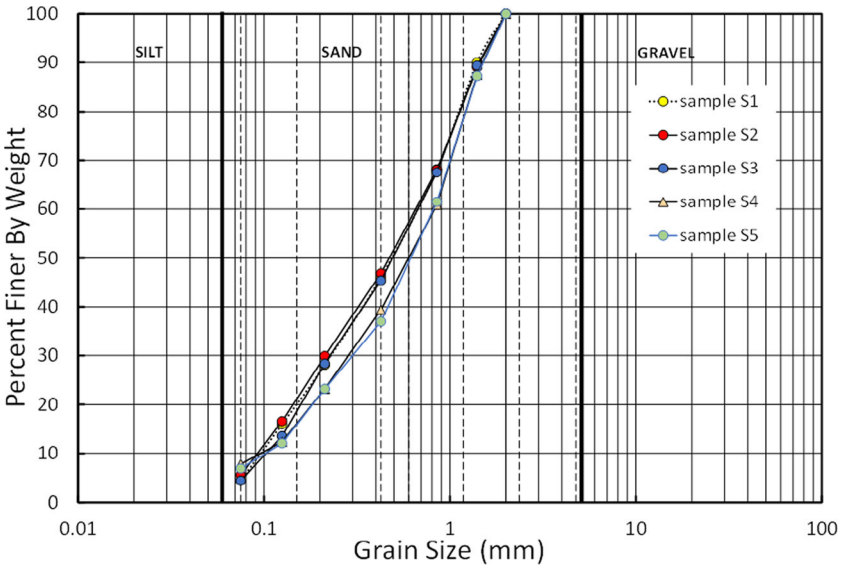

Fig. 6 Grain size distribution of samples collected from Donga Kass landslide

The general purpose of the DPRI ring-shear apparatus is to quantitatively simulate the entire process of failure of a soil sample, from initial static or dynamic loading, through shear failure, pore-pressure changes, and possible liquefaction, to large displacement, steady-state shear movement. No other laboratory apparatus has so far been able to provide an integrated simulation of this natural process. The latest devices in the DPRI ring-shear series have succeeded in this goal (Sassa et al. 2004).

Configuration and control system of ring shear apparatus

This initial landslide occurrence was geotechnically simulated using the DPRI-5 ring-shear apparatus. The apparatus is designed to study the mechanism of landslide motion and is sufficiently equipped to allow the speed and stress control tests along with measurement of a very large shear displacement (Sassa et al. 2003; Wang and Sassa 2001).

Figure 7a, b shows a schematic diagram of the apparatus and close half section of shear box, while Fig. 7c presents a brief illustration of the electrical control system of DPRI-5. The apparatus was installed in a pit at the DPRI Landslide laboratory with the level of the sample box approximately 1 m above the floor for easy access. Figure 7a illustrates concept of the ring-shear apparatus. Samples (disturbed) were taken from the layer where a sliding surface can be formed in the future. Then, the sample is set in the ring shear box including static upper half and a rotary lower half. All stresses acting on the potential sliding surface can be reproduced in the shear box such as normal and shear stresses due to gravity and seismic stress due to seismic shaking as well as generated pore-water pressures. When shear stress (static, seismic) is high enough to trigger sample failure, the rotary lower half of the shear box will start to turn. The annular ring-shaped sample will be sheared on a plane of relative rotary motion.

As shown in Fig. 7b, c, the sample is loaded by a loading platen through an oil piston (OP1), and the loaded normal force (for normal stress) is measured by a load cell (N1). The sum of the friction between the sample and the sidewall of the upper pair of rings in addition to the self-weight of the upper pair of rings is measured by a load cell (N2). The actual normal force acting on the shear surface is obtained from the difference between N1 and N2. This value is sent to a servo-amplifier as a feed-back signal (as shown in Fig. 7c). Then, the normal stress on the shear surface is automatically kept the same as the control signal given by the computer. Shear stress is supplied by a torque-controlled servomotor, which can be switched to a speed-controlled mode as well. The applied torque is measured by torque transducer T1. Using the monitored value of T1 as the feedback signal, the applied shear stress is automatically controlled by the servo-amplifier and servomotor and then kept the same as the pre-determined value given by the computer. The shear resistance acting on the shear surface is monitored by two load cells (S1 and S2), through which the upper shear box is restrained from rotation.

The most essential part of the undrained ring-shear apparatus is the undrained shear box. Its design is illustrated as Fig. 7b, an enlarged diagram of the left half of the cross section of the undrained shear box and its surroundings, including the water-pressure measurement system. Leakage of water through the gap between the upper shear box and the lower shear box was prevented by using stair-shaped rubber ring, rubber hardness index, 45°JIS ((Shoaei and Sassa 1994) as shown in Fig. 7b. In order to reduce friction and prevent water leakage, rubber edges were sprayed with Teflon spray and coated with silicon grease.

Testing procedure

The samples were formed by dry deposition method (as described by Ishihara 1993). Vaid et al. (1999) performed an experimental study and compare the behavior of truly undisturbed sand specimens retrieved by in situ ground freezing method and their corresponding reconstituted counterparts (dry deposition and moist tamping) after consolidating to identical initial states and found that the reconstituted specimens can be used as substitutes for the expensive undisturbed frozen specimens for material characterization. Another study was done by Sze and Yang (2014)

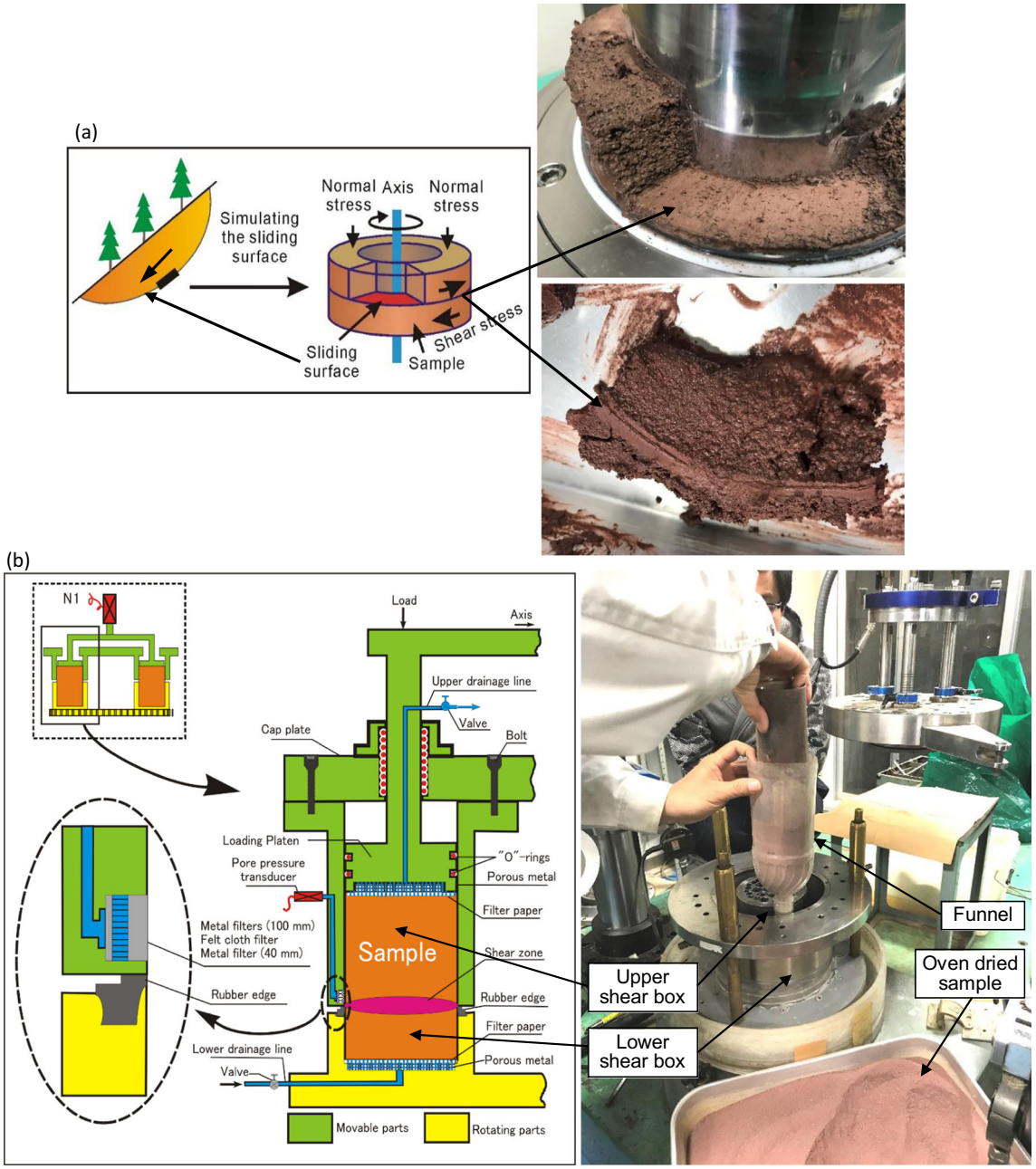

Fig. 7 **a** Concept of the ring-shear apparatus (left-modified from Sassa 2013) and photo showing sliding surface after testing (right). **b** A section of the ring shear box (version DPRI-5) and the close-up diagram of the edges (figure also shows the sample preparation by dry deposition method). **c** Electronic control system

to explore the impact of specimen preparation on the cyclic loading behavior of saturated sand by cyclic triaxial tests. They found that the soil fabric formed by dry deposition can lead to unique failure modes different from those of moist-tamped samples. These failure modes are hybrid in nature, characterized by a contractive response in the form of limited flow followed by cyclic strain hardening in the form of either cyclic mobility or plastic-strain accumulation. The 2005 Kashmir earthquake hit the region in the dry season, so dry deposition method was used to prepare the samples instead of moist tamping method. Moreover, dry deposition method can correlate soil formation history on site (the cyclic deposition of soil layers).

The oven-dried sample was compacted in six layers to form a specimen that was 180 mm in diameter and 115 mm in height. The funnel tip was maintained at a minimal height of drop above the soil surface. Tapping was then done uniformly around the periphery of the mold using a rubber rod to achieve a higher density (relative density, Dr. = 60%). The samples were saturated with the help of carbon dioxide and de-aired water. After the sample was packed, CO_2 was percolated through it to expel the air from the sample pores. The CO_2 was slowly introduced into the sample through the lower drainage line and discharged from the upper drainage line (Fig. 7b). Usually, this process took 4–12 h. After hours of percolation of CO_2, de-aired water was infiltrated into the

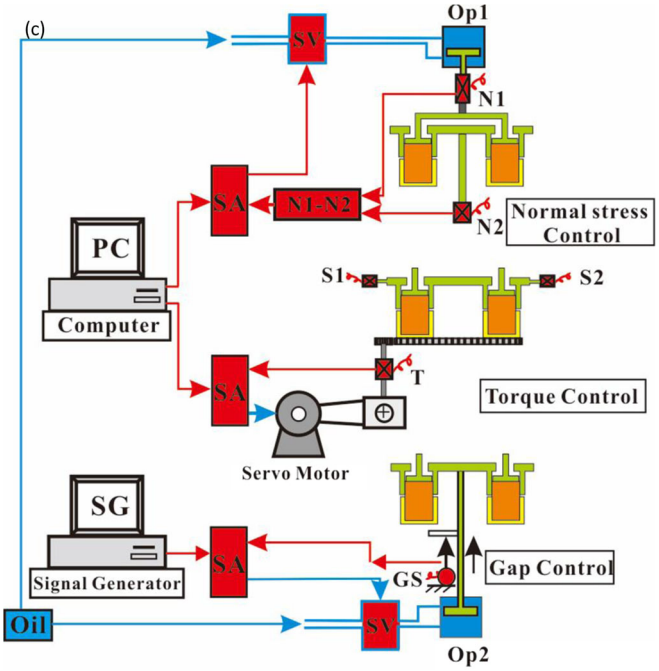

N1, N2: Load cell for normal stress; T: Load cell for torque;
S1, S2: Load cell for shear resistance; GS: Gap sensor;
OP: Oil piston; SV: Serve-oil valve; SA: Servo amplifier.

Fig. 7 (continued)

sample from the lower drainage line to expel the CO_2 in the sample pores from the upper drainage line. This infiltration process was kept at a very slow rate by using a very small water head. The degree of saturation was checked by using B_D value. B_D is a pore-pressure parameter, related to the degree of saturation in the direct-shear state, that was proposed by Sassa (1988), and is formulated as ($B_D = \Delta u/\Delta\sigma$) where Δu and $\Delta\sigma$ are increments of pore pressure and normal stress, respectively. Undrained tests were usually carried out with $B_D > 0.95$. In most cases, the soil layers in which sliding surfaces formed were weathered or fully softened. Therefore, the samples taken from the landslide sites were normally consolidated before the test. After checking the B_D value, the sample was consolidated and the initial shear stress due to the weight of the soil mass above the sliding surface was applied slowly to reproduce an initial stress state same as in situ conditions.

Additional seismic shaking or pore-pressure increase corresponding to rain storms was applied onto the sample in the undrained condition, or sometimes in the naturally drained condition, keeping the upper drainage valve open. Change of mobilized shear resistance is measured by two load cells (S1 and S2 shown in Fig. 7c). Pore pressure, resulting shear displacement, and shear speed were also monitored. The shear resistance mobilized during shearing was obtained by subtracting the rubber-edge friction from the monitored shear resistance.

Results and discussion

Pore pressure control test

The pore pressure control test was conducted to simulate the failure and the post failure behavior corresponding to rainfall in a naturally drained condition. This initial landslide occurrence was geotechnically simulated using the DPRI-5 ring-shear apparatus. The initial stresses on the sliding surface were reproduced in the apparatus; then, the pore water pressure (PWP) was gradually increased simulating the rise of ground water which would not be rapid; thus, the undrained loading condition was not used. To simulate drained ground-water conditions, water pressure supplied to the shear box through the upper drainage valve was gradually increased. Thus, water pressure was controlled, but the water was free to move through the upper valve. Therefore, the sample was subjected to a natural drained condition. If pore pressure was generated in the shear zone during loading, it drained naturally through the upper valve.

The hydrological triggering can be explained as the decrease in shear strength due to an increase of pore water pressure on the failure surface which results in a slope failure. Pore water pressure increase may be directly related to rainfall infiltration and percolation (saturation from above) or indirectly, as the result of built up of perched water bodies or a ground water table (Terlien 1998).

During the test, the sample was first saturated and then normally consolidated under a normal stress of 210 kPa. This preparatory stage was to reproduce the initial stress ($\sigma_\circ = \gamma D\cos^2\theta, \tau_\circ = \gamma D\cos\theta\sin\theta$) in the slope and is shown as a black line in Fig. 8a, where D is the depth of sliding surface and θ is the angle of sliding surface. This initial stress corresponds to a slope or arctan (97/210 = 25°) which is the slope of the sliding surface of landslide. Then, to simulate the pore pressure-induced landslide process, the pore water pressure was gradually increased at a rate of 1 kPa/s up to 210 kPa. Failure occurred at a pore water pressure of 78 kPa (a pore water pressure ratio $r_u = 78/210 = 0.371$). This is the critical pore water pressure ratio which can trigger the landslide without an earthquake. The friction angle at failure was 35.7°. The stress path is going down the failure line during motion with a friction angle of 33.8°. To monitor the water pressure during shearing, the pore water pressure supply valve was closed after failure occurred. After closing the pore water pressure supply valve, pore-water pressure increased with the progress of shearing, and shear resistance decreased correspondingly. When the shear displacement reached 1000 mm, the shear resistance arrived at an approximately constant value due to no additional increase in pore-water pressure, i.e., steady state (i.e., 45 kPa) was reached.

As shown in Fig. 8a, the effective stress path moved down along the failure line after failure. The stress path was that of typical sliding-surface-liquefaction (Sassa 1996, 2000). The grains in the shear zone were crushed during shearing and a high pore water pressure was generated by reduction of volume (Sassa et al. 2004, 2010; Doan et al. 2017).

Drained speed control test

Drained speed control tests were performed to check the shear rate effect on shear resistance; also, it is a basic test to measure the friction angle of a sample. First, the sample was saturated to B_D = 0.95, consolidated to different normal stresses (200, 250, 300 kPa) in the drained condition and then sheared at a constant rate of 0.05 cm/s. The results of the tests are presented in Fig. 9a showing the peak friction angle ($\phi_p = 35°$) and cohesion of 18 kPa. The lower graph in Fig. 9b shows the time series data for total normal stress, shear resistance, and pore pressure. Pore pressure remained zero throughout the test, since the test was under a

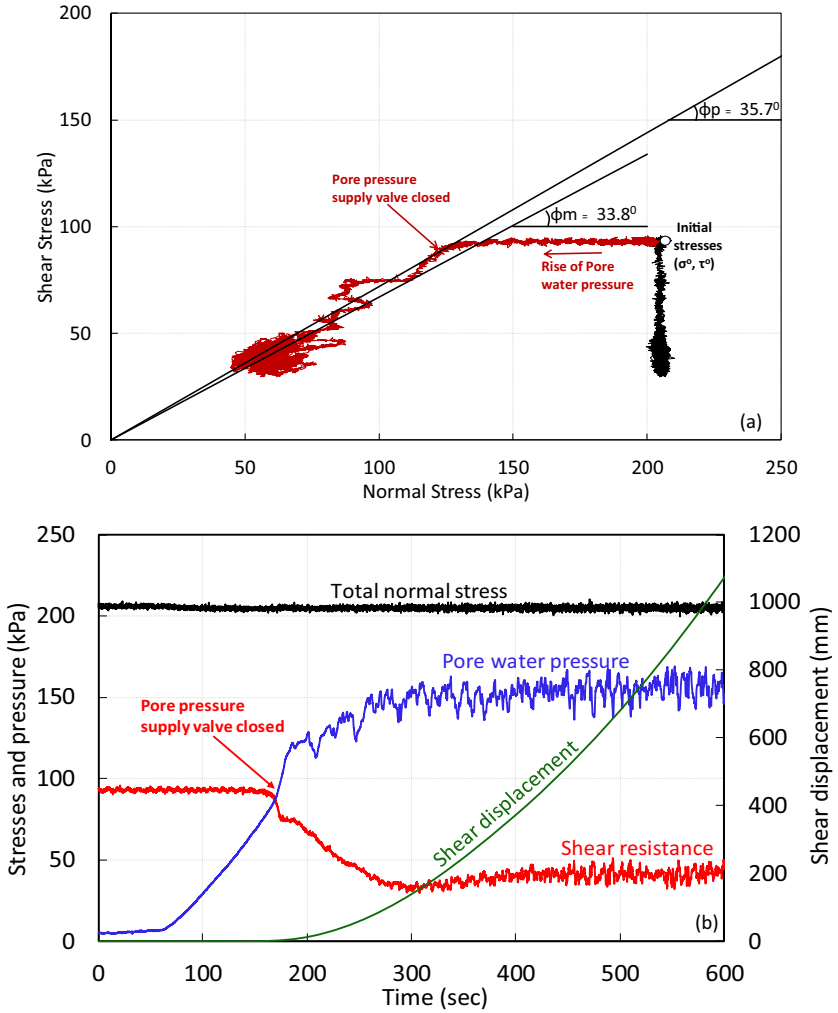

Fig. 8 **a** Stress path of pore pressure control test. **b** Time series data of pore pressure control test

drained condition. Figure 9c shows the relationship between volumetric strain and time. It shows the typical curves of volumetric strains observed at different normal stresses. It was observed that volumetric strains during drained shear tests depended upon normal stresses. Higher the normal stress, higher the volumetric sample strains/deformations were observed. Moreover, a contractant volume behavior was observed in all tests. All the samples showed sample vertical height reductions during the shearing phase. The decrease in volume was possibly caused due to particle crushing during shearing phase as described by Sassa et al. (2004). The stress path, friction angle and cohesion value appeared to be reasonable for the nature of the sample.

Undrained cyclic stress test

An undrained cyclic shear stress test was performed on the saturated sample to assess the acceleration required to cause the failure. Initial normal stress and shear stress corresponding to a depth of 15 m in a 25° slope were reproduced. The slope is in the projecting ridge; therefore, a high ground water level is not expected in the ordinary period without rainfall, while the bottom of the ridge (sand layer at the toe shown in Fig. 5a) is expected to be saturated due to river flow at the bottom. Initially, the saturated sample was consolidated at 210 kPa normal stress, then a 97 kPa shear stress was loaded in the drained state to create the initial stress state. The slope angle for this combination of normal and shear stresses corresponds to arctan (97/210 = 25°). The shear box was then switched to the undrained state for the undrained cyclic loading test, and after initial stresses were created by applying pre-decided normal and shear stress in the drained condition, dynamic cyclic loading was applied in an undrained condition. For all the undrained cyclic tests, one-way cyclic loading with constant amplitude of 30 kPa was loaded as 40 cycles of sinusoidal wave at the frequency of 0.5 Hz. A control signal (Fig. 10a) to produce the required cyclic shear stress by increasing its value up to 123 kPa ensured the occurrence of failure. As seen in the Fig. 10d, the mobilized maximum shear stress was about 101.5 kPa (which corresponds to a critical seismic acceleration of 175 gal) in the shear stress increment to cause failure from the following relation by Sassa et al. (2004).

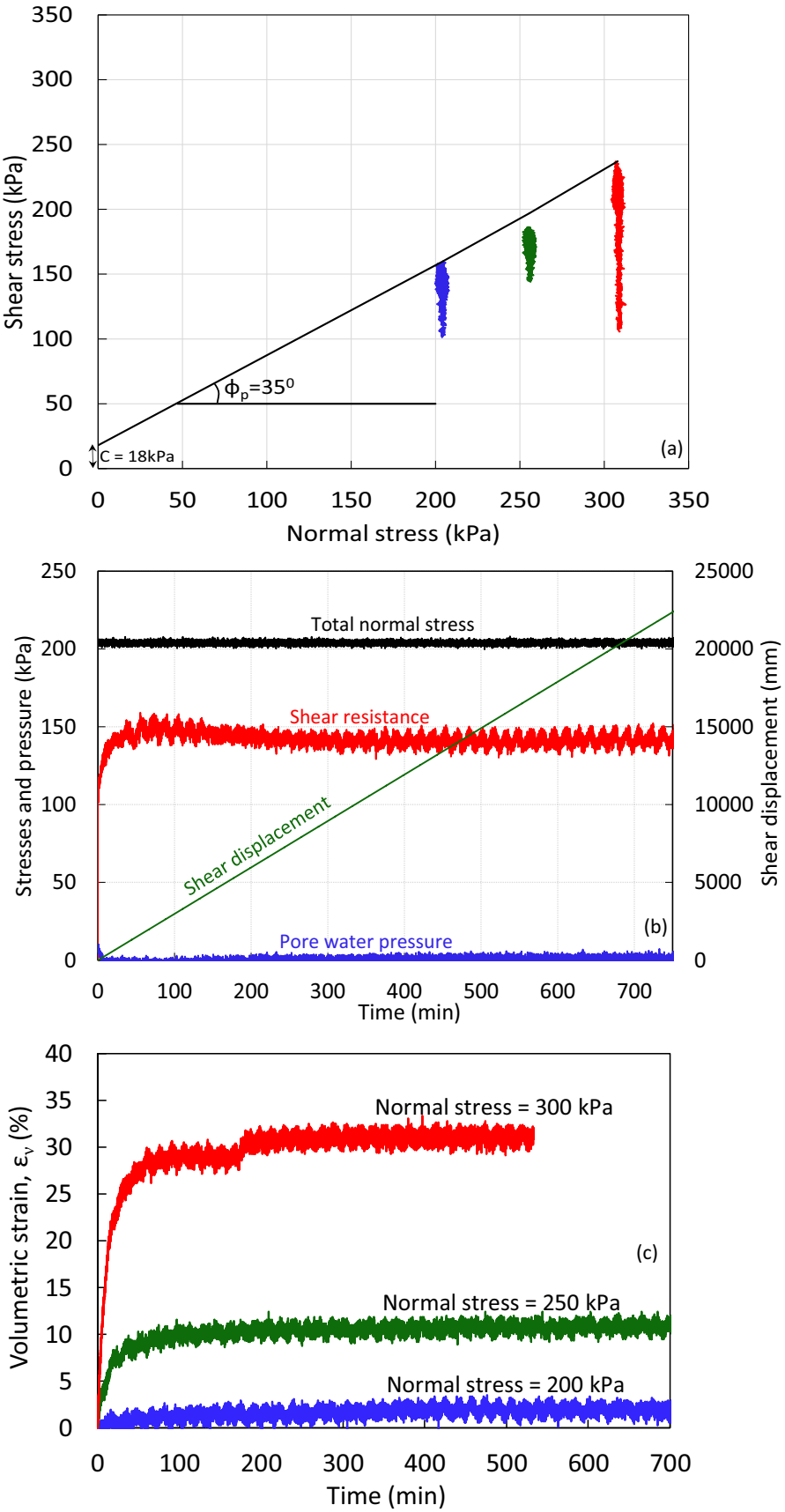

Fig. 9 **a** Drained shear test results on Donga Kass landslide ($B_D = 95\%$). **b** Time series data of drained ring shear test. **c** Rate of change of volumetric strain

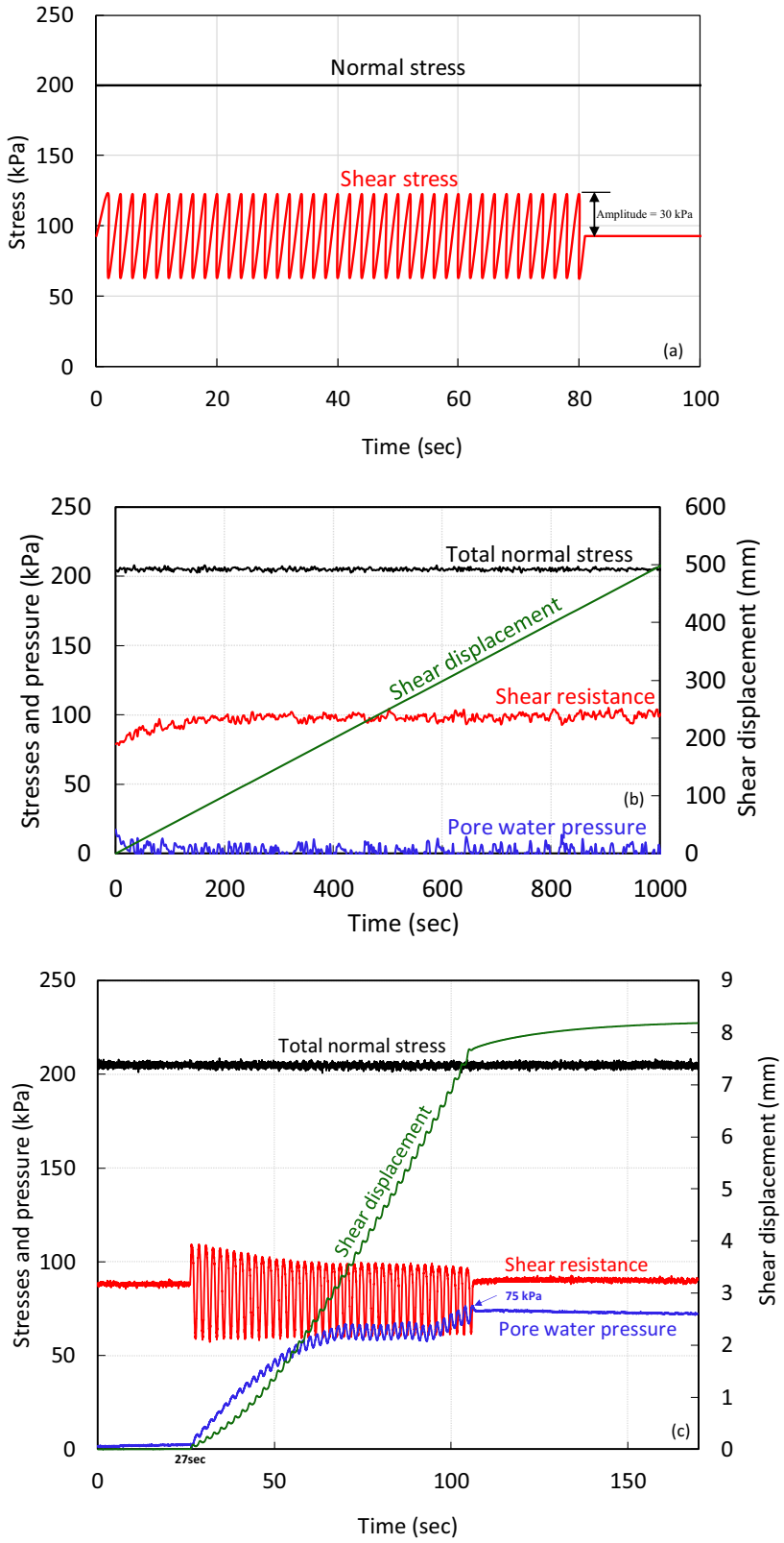

Fig. 10 **a** Control signal for normal stress and shear stress. **b** Time series data for the first run of cyclic loading. **c** Time series data for the second run of cyclic loading. **d** Time series data for the third run of cyclic loading. **e** Stress path of effective stress in undrained cyclic loading test

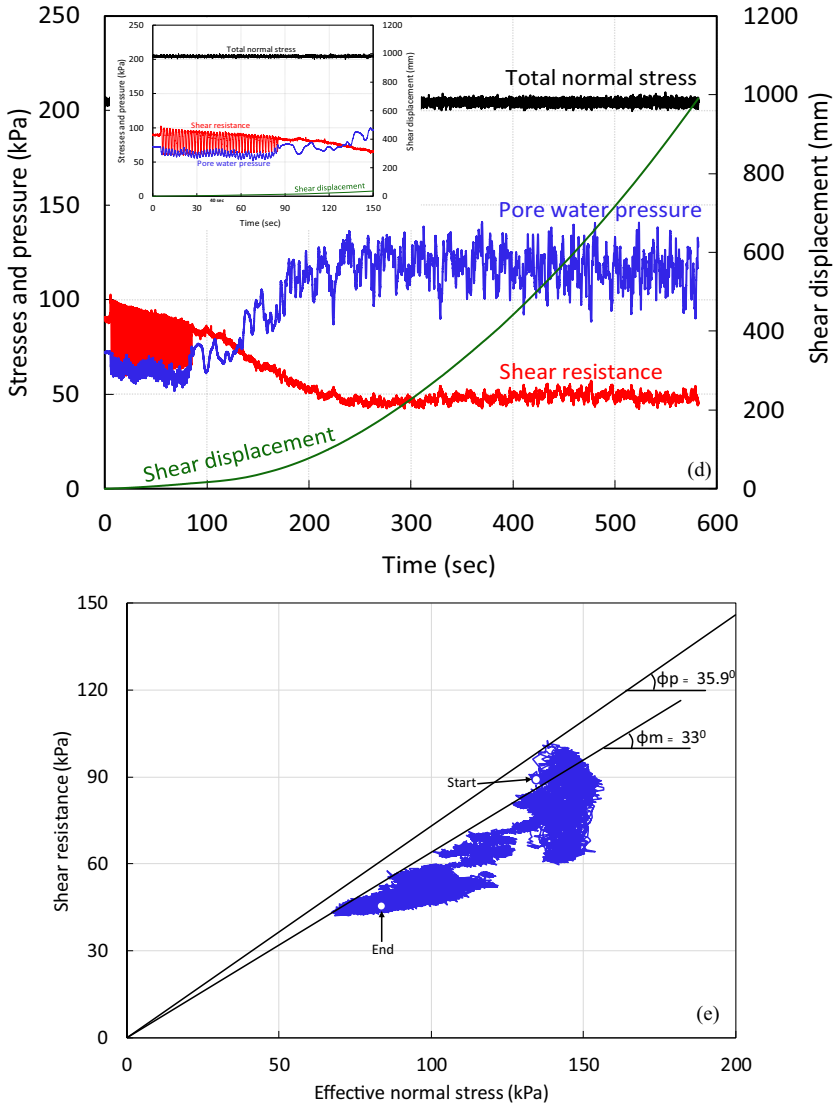

Fig. 10 (continued)

$$a_f = \left(\ \tau_f/m\right) = \left(\ \tau_f/\tau_o\right) \times \mathrm{gsin}\theta$$

where

m	mass of a unit column between the ground surface and the potential sliding surface
θ	angle of the potential sliding surface
τ_o	Initial shear stress due to self-weight of the column acting on the sliding surface
$\Delta\tau_f$	seismic shear stress increment required to cause failure (ma_f)
a_f	seismic acceleration to cause the above seismic shear stress

Undrained cyclic stress test was performed three times on the same soil sample as it did not fail in the first and second run of cyclic loading (each control signal loaded 40 cycles of sine waves). Figure 10b shows the time series data of the first run of the cyclic loading test. The red line shows the shear resistance mobilized on the sliding surface. The blue line shows pore water pressure and the green line shows the shear displacement. During the first run of cyclic loading after 40 sine waves, there was not a significant change in the shear resistance and no pore water pressure was generated. A shear displacement started to generate after 50 s and goes up to 500 mm.

There was no failure of soil observed in the first run of cyclic loading. Therefore, the same control signal with 40 sine waves was loaded to the soil sample. During the second run of cyclic loading shown in Fig. 10c after the first 27 s, the pore water pressure starts to generate and goes up to 75 kPa then become steady and at the same time shear displacement begins to increase, goes up to 7 mm, and then becomes steady. There was no significant decrease in the shear resistance and no failure of the soil.

The control signal with 40 sine waves was loaded third time to the soil sample. During the third run of cyclic loading (Fig. 10d) showed pore water pressure generation after 40 s, failure of soil specimen and further increase of pore water pressure with the progress of shear displacement which results in reduction of shear resistance until a steady-state shear strength of 45 kPa. This phenomenon is referred to as 'Sliding surface liquefaction" as described by Sassa et al. (2004). The peak friction angle is 35.9° and mobilized friction angle is 33° as shown in the Fig. 10e. The accelerated motion was produced after failure of the soil. Shear resistance was suddenly decreased down to the steady state of the shear resistance though the control signal was stopped. Motion is accelerated even after cessation of cyclic loading and stopped after reaching 1000 mm.

According to Sze and Yang, the specimen prepared by dry deposition (DD) during cyclic loading test exhibited a contractive response in the initial stage of shear that was then followed by a dilative, strain-hardening response to large deformation. On the other hand, at the same density and confining stress, there was no such hardening response in the specimens prepared by moist tamping (MT), and the cyclic-loading test resulted in complete flow failure. Figure 10c shows the results of the second undrained cyclic loading series, the PWP and shear resistance became steady after about 100 s, which could suggest that the soil may have reached a steady state. The subsequent third loading series suddenly triggered a tremendous build-up of pore water pressure (and hence reduction of shear resistance) as shown in Fig. 10d. A sudden rise in PWP is associated with the occurrence of the sudden deformation followed by a drop of effective stress. At a medium-dense state (relative density, Dr. = 60%) with sufficient stress reversal in cyclic loading, the failure herein referred to "limited flow" behavior of sand, observed by Sze and Yang (2014). The triggering of flow was related to the occurrence of strain softening, but the flow was limited because of the associated strain hardening response in the subsequent shear.

Conclusion

- Landslide risk analysis for a rapid landslide triggered by rainfall and earthquake was conducted using data obtained by ring shear tests on samples together with geological and topographical investigation of the study site. The results of the investigation show that the landslide could be subjected to sliding surface liquefaction with resulting rapid rainfall induced landslide in the future. Therefore, corrective countermeasures should be taken for the Donga Kass landslide.
- Donga Kass landslide was activated during the 2005 Kashmir earthquake in northern Pakistan causing many causalities and blocked the Neelum valley road for several days. The factors controlling the landside activity includes steep slope, presence of silty and clayey material, construction of the Neelum road and river under cutting along with rainfall and seismo-tectonic activity.
- This is a preliminary study which elevates the understanding on the landslide phenomena and the triggering factors at the Donga Kass landslide. But this is based on limited field and laboratory testing observations, as landslide perdition is required a more comprehensive analysis along with the design of some suitable countermeasure (such as design of proper drainage system so that pore pressure would not be built up in the landslide mass or implementation of some bioengineering technique) in the future. The current research can be a base for further study in the future for the landslide prediction and design of suitable remedial measure for the landslide.
- The study area is tectonically active, also it experienced extreme monsoon rainfall each year. During the field investigation, it was observed that the rock units were badly sheared, fractured, and deformed with tension cracks of 15 cm to 1.5 m wide and 1 m deep. It will be very fragile to any future tectonic activity.
- During field observation, it was recognized that the Donga kass landslide was a translational type of slide and the slip surface was not exposed and had been covered by debris. There were lot of vertical joints (fractures) on the weathering crust about 1–5 m thick. These fractures allow water and surface moisture to penetrate the rock and weaken sandstone, siltstone, and the shale layer, causing an increase in weight, reducing the bonding strength between two layers and thus promoting failure.
- The sample showed stress reversal in cyclic loading test, the triggering of flow was related to the occurrence of strain softening, but the flow was limited because of the associated strain hardening response in the subsequent shear during the third cycle of loading. The failure herein referred to "limited flow" behavior of sand, observed by Sze and Yang (2014).
- Based on the conducted pore pressure control tests, it is suggested that a pore pressure ratio of 0.371 could have caused the landslide without an earthquake. Using this value and combining with rainfall data and monitored pore water pressure in bore holes, the time of this landslide can be predicted, thereby reducing landslide risk by using early warning system.
- A cyclic loading ring shear test was performed three times on the silty sand specimen from the Donga Kass slide, in the first and second run of cyclic loading, there was no soil failure, whereas failure happened after applying a third run of cyclic loading indicating that the Donga Kass soil is resistant to seismic loading.
- This study provided considerable insight into the landslide activation phenomenon. Every year, a considerable amount of road maintenance budget is allocated to repair the road after the monsoon season (i.e., July to August). Hence, a detailed analysis for effective countermeasures considering the failure mode (i.e., excess pore pressure ratio criteria for rainfall induced landslide) would not only be helpful in reducing the invaluable human lives lost but also will result in saving a considerable amount of money allocated as a maintenance budget every year.

Acknowledgements

We appreciate the assistance of our colleagues at Prof. Takara's Laboratory especially Mr. Hendy Setiawan, Ms. Sono Inoue and Ms. Kaori Saidera. The first author gratefully acknowledges the valuable review and comments by Prof. James Goltz, a Visiting Professor in DPRI, who proofread the paper. We thank the anonymous reviewers whose comments have greatly improved this manuscript. The first author deeply appreciates the cooperation of all the members of the Planning and Development Department and the Central Design Office of Muzaffarabad, Azad Jammu and Kashmir for providing valuable data and information for our field visit. The author would like to express

her heartfelt gratitude to Mr. Muhammad Shehzad Khalid, a PhD Student at Kyoto University for his assistance during site investigation and sampling from the landslide. Special thanks to Khawaja Shoaib Ahmad, an M.Phil. student at the Institute of Geology, University of Azad Jammu and Kashmir for preparing geological cross sections of the landslide.

Funding information

The financial support for this project was provided by the Disaster Prevention Research Institute (DPRI) of Kyoto University, Japan.

References

Baig MS, Yeats RS, Monalisa (2008) Active deformation, fault segmentation, scarp morphology, seismic hazard assessments and geohazards along Muzaffarabad fault, Hazara Kashmir Syntaxis northwest Himalaya Pakistan, international seminar on "earthquake hazards Pakistan: post-October 2005, Muzaffarabad Earthquake Scenario, pp. 8–10

Basharat M, Rohn J, Baig MS, Ehret D (2012) Lithological and structural control of Hattian Bala rock avalanche triggered by the Kashmir earthquake 2005, NW Himalaya, Pakistan. J Earth Sci 23(2):213–224

Basharat M, Yasir S, Khawaja SA, Muhammad ZA (2017) A preliminary investigation of reactivated mass movement near the epicenter of 2005 Kashmir earthquake, NW Himalayas, Pakistan. JHES 50(1A):57–65

Bishop AW, Green GE, Garga VK, Andersen A, Brown JD (1971) A new ring-shear apparatus and its application to the measurement of residual strength. Geotechnique 21(1):273–328

Bromhead EN (1979) A simple ring-shear apparatus. Ground Eng 12(5):40–44

Doan HL, Quang LH, Sassa K, Takara K, Dang K, Nguyen KT, Tien PV (2017) The 28 July 2015 rapid landslide at Ha Long City, Quang Ninh, Veitnam. Landslides 14(3):1207–1215

Earthquake Reconstruction and Rehabilitation Authority (EERA), http://www.erra.pk/. Accessed 20 Jan 2018

Garga VK, Sendano JI (2002) Steady state strength of sands in a constant volume ring-shear apparatus. J Geotech Test 25(4):414–421

Hufschmidt G, Crozier M, Glade T (2005) Evolution of natural risk: research framework and perspectives. Nat Hazards Earth Syst Sci 5:375–387

Hungr O, Morgenstern NR (1984) High-velocity ring-shear tests on sand. Geotechnique 34(3):415–421

Hussain A, Iqbal S, Nasir S (2004) Geological maps of the Garhi Habibullah and Nauseri area, district Muzaffarabad, AJK, geological survey of Pakistan. Prelim Map Ser 4(14), Sheet No. 43 F/7,11, 1:50,000

Hvorslev MJ (1939) Torsion shear tests and their place in the determination of the shearing resistance of soils. Proc Am Soc Test Mater 39:999–1022

Ishihara K (1993) Liquefaction and flow failure during earthquakes. Geotechnique 43(3):349–451

Kaneda H, Nakata T, Tsutsumi H, Kondo H, Sugito N, Awata Y, Akhtar SS, Majid A, Khattak W, Awan AA, Yeats RS, Hussain A, Ashraf M, Wesnousky SG, Kausar AB (2008) Surface rupture of the 2005 Kashmir, Pakistan earthquake and its active tectonic implications. Bull Seismol Soc Am 98:521–557

Khattak GA, Owen LA, Kamp U, Harp EL (2010) Evolution of earthquake-triggered landslides in the Kashmir Himalaya, northern Pakistan. Geomorphology 115 (1-2):102–108

Konagai K, Sattar A (2011) Partial breaching of Hattian Bala landslide dam formed in the 8th October 2005 Kashmir earthquake, Pakistan, landslides, vol. 9, pp. 1–11

Petley D, Dunning S, Rosser N, Kausar AB (2006) Incipient landslides in the Jhelum Valley, Pakistan following the 8th October 2005 earthquake. Disaster mitigation of rock flows, slope failures and landslides by universal. Academy Press, pp. 1–9

Planning and Development department Azad Jammu and Kashmir, AJK at a glance (2015) http://ajk.gov.pk. Accessed 05-08-2016

Saba SB, Meijde VDM, Werff VDH (2010) Spatiotemporal landslide detection for the 2005 Kashmir earthquake region. Geomorphology 124:17–25

Sassa K (1984) The mechanism starting liquefied landslides and debris flows, proceedings of 4th international symposium on landslides, Toronto, June, Vol.2, pp. 349–354

Sassa K (1988) Motion of landslides and debris flows-prediction of hazard area. Report for Grant-in-aid for scientific research by Japanese ministry on education, science and culture (project no. 61480062), pp. 15

Sassa K (1994) Development of a new cyclic loading ring-shear apparatus to study earthquake-induced-landslides, report for grain-in-aid for developmental scientific research by the Ministry of Education, science and culture, Japan (Project No. 03556021), pp. 106

Sassa K (1996) Prediction of earthquake induced landslides. Proceedings of 7th International Symposium on Landslides, A.A. Balkema. Trondheim, 17–21 June, vol.1, pp. 115–132

Sassa K (2000) Mechanism of flows in granular soils, Proceedings of Geo Eng 2000, Melbourne, vol.1, pp. 1671–1702

Sassa K, Wang G, Fukuoka H (2003) Performing undrained shear tests on saturated sands in a new intelligent type of ring shear apparatus. Geotech Test J 26(3):257–265

Sassa K, Fukuoka H, Wang G, Ishikawa N (2004) Undrained dynamic-loading ring-shear apparatus and its application to landslide dynamics. Landslides 1(1):7–19

Sassa K, He B (2013) Landslide initiation mechanism,TXT-Tool 3.081-1.1, ICL Landslide Teaching Tools, pp. 205–213

Sassa K, Nagai O, Solidum R, Yamazaki Y, Ohta H (2010) An integrated model simulating the initiation and motion of earthquake and rain induced rapid landslides and its application to the 2006 Leyte landslide. Landslides 7(3):219–236

Savage SB, Sayed M (1984) Stresses developed in dry cohesionless granular materials sheared in an annular shear cell. J Fluid Mech 4(2):391–430

Shoaei Z, Sassa K (1994), Basic study on the shear behavior of landslides during earthquakes excess pore pressure in the undrained cyclic loading ring-shear tests, Disaster Prevention Reseach Institute, Kyoto University Vol. 44(1), pp. 1–43

Sze HY, Yang J (2014) Failure modes of sand in undrained cyclic loading: impact of sample preparation. J Geotech Geoenviron Eng ASCE 140(1):152–169

Terlien MT (1998) The determination of statistical and deterministic hydrological landslide triggering thresholds. Environ Geol 35(2):124–113

Tika TM (1989) The effect of rate of shear on the residual strength of soil, PhD Thesis, University of London (Imperial College of Science and Technology), pp. 494

Vaid YP, Sivathayalan S, Stedman D (1999) Influence of specimen reconstituting method on the undrained response of sand. ASTM Geotech Test J 22(3):187–195

Wang G, Sassa K (2001) Factors affecting rainfall induced flowslides in laboratory flumes tests. Geotechnique 51(7):587–599

World Bank (2005), https://www.worldbank.org/ and Asian Development Bank (2005), https://www.adb.org/. Accessed 22 Jan 2018

S. Riaz (✉) · **G. Wang** · **K. Takara**
Disaster Prevention Research Institute,
Kyoto University,
Kyoto, Japan
Email: saimariaz04@gmail.com

G. Wang
e-mail: wanggh@landslide.dpri.kyoto-u.ac.jp

K. Takara
e-mail: takara.kaoru.7v@kyoto-u.ac.jp

M. Basharat
Institute of Geology,
University of Azad Jammu and Kashmir,
Muzaffarabad, Pakistan
e-mail: basharatgeo@yahoo.com